BIII-4

CRACK RESISTANCE PROPERTIES OF HIGH STRENGTH ALUMINUM ALLOYS

C. M. Carman[1], D. F. Armiento[1] and H. Markus[2]

ABSTRACT

The principles of fracture mechanics define the critical value of $\mathcal{G}$ as that value of crack tip driving force necessary to produce crack instability. The concept of crack instability is discussed, using the relationship of the partial derivative $\partial\mathcal{G}/\partial a$ with respect to "a" (half crack length) and the partial derivative of R (material resistance) with respect to "a". Instability occurs when the rate of change of stress with specimen elongation is zero ($d\sigma/de = 0$).

In ordinary fracture toughness testing, only one point on the crack resistance curve is determined; namely, the instability point, $\mathcal{G}_c$, for the particular specimen used. However, it has been shown that $\mathcal{G}_c$ is sensitive to geometrical effects, and so it is necessary to develop the full crack resistance curve of the material to explain the plane stress fracture behavior.

Experimental data obtained for the high strength aluminum alloys of the Al-Zn-Mg family (7000 series) show that these materials exhibited limited slow crack extension. Comparison of the data obtained with 4-in. and 20-in. wide panels showed somewhat higher $\mathcal{G}_c$ values for the 20-in. wide panel tests and that the wider panels are necessary to more fully develop the crack resistance curve.

Experimental data obtained for high strength aluminum alloys of the Al-Cu family (2000 series) and a strain hardening alloy (5456-H343) show that these materials exhibited considerable slow crack extension. However, due to their higher fracture toughness and lower strength, it was possible to develop only the initial portion of the crack resistance curve.

---

(1) Mr. C. M. Carman and Mr. D. F. Armiento are Metallurgists, Pitman-Dunn Research Laboratories, Frankford Arsenal, Philadelphia, Pennsylvania, U. S. A.

(2) Mr. H. Markus is Director, Metallurgy Research Laboratory, Frankford Arsenal, Philadelphia, Pennsylvania, U. S. A.

The effect of purity on the fracture toughness of high strength aluminum alloys was studied using special melts of 7075-T6 and 2024-T4 having very low contents of iron and silicon. Results of this study show that increasing the purity increases the fracture toughness. A possible mechanism for this increase of fracture toughness is presented. This mechanism is based on the development and growth of the ductile rupture dimples observed on the fracture surface as influenced by the structure of these alloys.

LIST OF SYMBOLS

K = stress field parameter describing the local elevation of the elastic stress field ahead of the crack.

σ_{ox} = stress parallel to the crack.

E = Young's Modulus.

$\mathcal{B}$ = elastic energy release rate.

γ = Poisson's ratio.

R = crack resistance.

e = specimen deflection.

a = 1/2 crack length.

v = displacement in the y direction.

W = specimen width.

ε = strain.

σ_{net} = net section stress.

σ_{ys} = 0.20 percent tensile yield strength.

σ = gross section stress.

WPZ = with plastic zone correction.

WOPZ = without plastic zone correction.

dW/dA = work function.

y = distance from the crack plane at which displacement measurements were made.

Subscripts

I = first or opening mode of fracture.

c = critical value of a parameter.

INTRODUCTION

In a recent article, Irwin and Srawley[1] have reviewed the current status of fracture testing in relation to materials evaluation, using the concepts of modern fracture mechanics. In their review, fracture mechanics was defined as a branch of classical mechanics of deformable media which deals with bodies containing cracks. Irwin,[2] in a detailed explanation of the subject, has defined the crack in the mathematical model as a flat internal free surface in an elastic solid. He directed attention to the elastic stress field which surrounds the crack when a body is subjected to any distribution of forces or loads. To avoid unnecessary complexities, consideration was centered on the stress field at the leading edge of the crack. By means of an appropriate stress analysis, it is possible to express the effects of component shape and loading conditions by a stress singularity at the leading edge of the crack. By this procedure, it is possible to describe the stress environment around the leading edge of the crack in terms of a single parameter, the crack edge stress field intensity, K.

The K parameter is directly related to the elastic energy release rate, or crack extension force, $\mathcal{G}$, of the theory of A. A. Griffith, as shown in Equations 1 and 2.

$$K^2 = E\mathcal{G} \quad \text{(plane stress)} \tag{1}$$

$$K_I^2 = \frac{E\mathcal{G}_I}{(1-\gamma^2)} \quad \text{(plane strain)} \tag{2}$$

From early considerations of the Irwin-Griffith concept, it would be anticipated that a relatively constant value of the critical elastic energy release rate, $\mathcal{G}_c$, would be obtained, regardless of specimen width. This value would be essentially independent of the crack length, "a", as illustrated in Figure 1A. In this figure the crack resistance of the material is shown as a constant or slightly decreasing value when plotted against the crack length, while the driving force curve is shown as an increasing function of "a". Instability will occur at the intersection of these two curves. At this point the two curves sharply diverge and result in a spontaneous oversupply of driving force for the crack.

However, experimental data obtained using specimens of various widths show that the above situation does not occur and that the wider, more deeply notched specimens show higher values of $\mathcal{G}_c$.[3]

Irwin[4] has advanced two concepts to explain the observed increase of fracture toughness with specimen width. Plastic deformation associated with crack growth is essential to the explanation for the difference of actual fracture energy requirements over surface free energy. In this analysis, it is assumed that this plastic deformation forms a zone of relieved tensile stress immediately ahead of the crack in the plane of the sheet, so that the crack is effectively longer than its actual extent. A roughly constant effective extension of a short crack, as in a narrow specimen, produces a relatively larger disturbance both on the stress field and on the $\mathcal{G}_c$ value, than that of a long crack in a wide specimen. It was hoped that constancy of fracture toughness as a material characteristic might be obtained by this method.

The second concept states that the plastic zone and, thus, the fracture toughness grow as the crack extends from a crack simulating machined notch or from an actual fatigue crack. This concept presents the possibility that the fracture toughness, at instability, need not be constant and that instability may occur before an equilibrium maximum size of the plastic zone is attained. If one describes the growth of fracture resistance, R, as a simple convex upward curve from the initial crack, a_o, to a limiting level (Figure 1B), fast fracture instability occurs at the point of tangency between it and the crack extension force curve, $\mathcal{G}$.

This concept is somewhat oversimplified in that the equality $\mathcal{G} = R$ is very nearly true for $\mathcal{G} > \mathcal{G}_c$ as well as $\mathcal{G} < \mathcal{G}_c$. Also, it should not be inferred that the difference between $\mathcal{G}$ and the extrapolated R curve is available to accelerate the crack. When $\mathcal{G} > \mathcal{G}_c$, the crack speed rapidly adjusts to a value such that the energy dissipation rate R equals the rate of energy supply $\mathcal{G}$. The R values to be subsequently described in this paper are the crack resistance values for nearly zero crack speed.

Srawley and Brown[5] have clarified the conditions for crack instability. By definition, $\mathcal{G}_c$ is equal to the value of R at instability, and beyond this point $\mathcal{G}$ increases more rapidly with specimen deflection, e, than does R. The values of $\mathcal{G}$ and R are equal up to the point of instability; these quantities represent distinctly different physical entities and have different functional relations to the subsidiary test variables σ and "a". The crack resistance of the material will follow the applied $\mathcal{G}$ at least up to the point of instability. Expressing this in terms of the subsidiary variables, σ and "a", yields

$$d(\mathcal{G} - R)/de = 0 = (\partial \mathcal{G}/\partial\sigma)(d\sigma/de) + (\partial \mathcal{G}/\partial a)(da/de) - (\partial R/\partial\sigma)(d\sigma/de) - (\partial R/\partial a)(da/de) \quad (3)$$

One definition of instability is $d\sigma/de = 0$ and, in that case, Equation 3 reduces to

$$(\partial \mathcal{G}/\partial a)_\sigma = \sigma_c = (\partial R/\partial a)_\sigma = \sigma_c \quad (4)$$

In a fracture toughness test as normally conducted, the value of only one point on the crack extension resistance curve is determined, namely, the instability point for the particular specimen used, which is called $\mathcal{G}_c$. How nearly independent of crack length $\mathcal{G}_c$ will be for a group of tests on the same material, using specimens with different initial crack lengths, will depend upon the form of the R curve for the material. To characterize the fracture toughness of a material thoroughly, it will be necessary to determine the entire R curve.

This investigation was undertaken to study and to develop the crack resistance curves of commercial high strength and high purity-high strength aluminum alloys.

MATERIALS

Precipitation hardening alloys of the Al-Zn-Mg family (7000 series) and the Al-Cu family (2000 series), procured as commercially rolled sheet, were selected for this investigation. A list of the various alloys and sheet thickness is shown in Table I.

Work in the ferrous industry has shown that improvement in the fracture toughness at high strength levels may be achieved by improving the purity of the products. This has resulted in the application of consumable electrode vacuum-melted steels for highly stressed parts. Assuming a similar effect may occur in aluminum alloys, high purity 7075 and 2024 aluminum alloys were melted from specially selected raw materials to produce alloys having very low impurity contents (max. residual impurities 0.025 percent). Comparison of the crack resistance curves of these materials with those of commercial alloys will permit assessing the effects of impurities on fracture toughness.

The engineering tensile properties of these alloys were determined using pin-loaded sheet specimens, 0.500 in. wide having a 2 in. gage length. Results are given in Table II. It will be observed that the tensile properties of the commercial and high purity alloys are within the normal commercial specification requirements for these alloys.

EXPERIMENTAL PROCEDURES

The development of the crack resistance curves requires a knowledge of the history of the stress and crack length up to the point of instability. Two experimental techniques are available for determining the stress and crack length relationship. The first technique involves direct measurement of the crack length and load during test. The second technique is concerned with the indirect measurement of crack length through the measurement of the change in the elastic compliance of the specimen. Both experimental procedures were used in this investigation.

The direct measurement technique can readily be applied to tests of relatively wide panels. The specimen employed for this phase of the investigation is shown in Figure 2. A specimen width of 20 in. for the reduced section was selected for all tests. After a preliminary study, an initial crack length of 8 in. was selected as giving the most information concerning the crack resistance curve. The specimens were machined to the desired contour, and the 8-in. slot was cut in the center by electro discharge machining. An additional sharper notch was cut at the tip of the slot by electro discharge machining using 0.0015 in. thick foil. This procedure results in a square notch tip of approximately 0.003 in. width. This tip was sharpened to a root radius of 0.001 in. by means of a hardened steel razor blade. Kaufman[6] has shown that this notch sharpness is equivalent to fatigue cracking for most high strength aluminum alloys.

General consideration of the shape of the crack resistance curve by Krafft, Sullivan, and Boyle[3] indicates an almost vertical rise of the crack resistance curve until plane strain instability is reached, followed by a development of greater crack resistance with crack growth. The initial onset of crack growth at plane strain instability cannot usually be detected on the surface of the specimen. To determine the crack pop-in load, electrical resistance strain

gages were attached to the specimen just ahead of the notch. When plane strain instability is reached, there is a rapid transfer of load so that an inflection is observed in the load-strain gage reading curve at crack pop-in.

The wide panel tests were conducted on a 300,000-lb tensile machine. These specimens were pin-loaded through special adaptors. Lubricated face plates were used to prevent buckling during the test. An assembled specimen is shown in Figure 3.

The crack length and load were recorded by means of two high speed motion picture cameras. One camera recorded the crack length and the other photographed the loading dial. The relationship between the two motion picture films was established by synchronized stop watches on the specimen and loading dial. The complete experimental equipment is shown in Figure 4.

An illustrative frame from the motion pictures, showing the crack length just preceding instability for 1/8 in. thick 7075-T6 aluminum, is shown in Figure 5.

The indirect method of crack length measurement involves detection of the change in elastic compliance of the specimen with crack extension. In essence, the technique consists of measuring the displacement of two fiducial points which span the crack and relating this to the crack extension.

The specimen selected for this phase of the investigation was a center-cracked specimen, 4 in. wide by 12 in. long. A center slot, 1 in. long, was cut in the specimen with a fine saw blade. The notch was precracked in fatigue prior to testing. The compliance gage used was similar to that described by Boyle[7] and consists of two L-shaped arms which are pivoted on the line of crack extension. An extensometer is attached to the end of the arms to measure the deflection. This instrument, in position on the specimen, is shown in Figure 6.

Irwin has derived an equation which relates the displacement and crack length. This expression is given in Equation 5.

$$\frac{Ev}{\sigma W} = \left\{\frac{2W}{\pi y}\cosh^{-1}\left(\frac{\cosh\frac{\pi y}{W}}{\cos\frac{\pi a}{W}}\right) - \frac{1+\gamma}{\left[1+\left(\frac{\sin\frac{\pi a}{W}}{\sinh\frac{\pi y}{W}}\right)^2\right]^{1/2}} + \gamma\right\}\frac{y}{W} \qquad (5)$$

Equation 5 was solved for a 4-in. wide panel and the values of $Ev/\sigma W$ are plotted as a function of $\pi a/W$ in Figure 7.

Although a theoretical relationship may be suitable for this purpose, it should be confirmed experimentally. Consequently, a series of 7075-T6 aluminum panels, 1/8 in. thick, with carefully machined slots of varying lengths, was prepared. These specimens were stressed at a low level to minimize the effect of plastic deformation at the slot tip. The experimentally determined relationship between displacement and crack length is shown as a solid curve in Figure 7.

It will be observed that the general shape of the curves is the same, although some significant differences were found. Wider divergence between the two curves was observed at $\pi a/W$ values greater than 0.8. This indicates that the boundary conditions assumed in the stress analysis do not apply for total crack lengths (2a) greater than W/2. Therefore, all data from specimens which had crack lengths at instability greater than W/2 were discarded. Also, in view of these discrepancies, although small, the experimentally determined curve was used in preference to the theoretical calibration curve for crack length measurements.

EXPERIMENTAL RESULTS AND DISCUSSION

This investigation may be divided into two parts. The first part is concerned with the definition and determination of crack instability. The second part is the actual development of the crack resistance curve. However, these two parts are not separable.

In the introduction, the point of instability was defined by Equation 4 to be $(\partial \mathscr{D}/\partial a)_{\sigma = \sigma_c} = (\partial R/\partial a)_{\sigma = \sigma_c}$. Use of this criterion requires the differentiation of the crack resistance curve and the crack driving force curve. The crack resistance curves were calculated from the instantaneous load and direct or indirect crack length measurements using Irwin's tangent formula:

$$\frac{dW}{dA} = R = \mathscr{D} = \frac{\sigma^2 W}{E}\tan\frac{\pi a}{W} \qquad (6)$$

The $(\partial R/\partial a)_{\sigma = \sigma_c}$ is determined by graphical differentiation of the crack resistance curve.

The value of half crack length at which the two derivatives are equal determines the critical value of $\mathcal{G}$. Since $\mathcal{G}$ is also defined by Equation 6, the value of $(\partial \mathcal{G}/\partial a)_\sigma = \sigma_c$ is determined by differentiating Equation 6 with respect to "a", resulting in Equation 7:

$$\frac{\partial \mathcal{G}}{\partial a} = \frac{d \mathcal{G}}{da} = \frac{\pi \sigma^2}{E} \sec^2 \frac{\pi a}{W} \tag{7}$$

Multiplying Equation 7 by $W/\mathcal{G}$ gives

$$\frac{d \mathcal{G}}{da} \left(\frac{W}{\mathcal{G}} \right) = \frac{2\pi}{\sin \frac{2\pi a}{W}} \tag{8}$$

The values of the derivatives of the crack resistance curve and the driving force curve will be plotted as a function of "a" on the same graph (e.g. Figure 9). The point of intersection of these two curves represents the half crack length at crack instability.

High Strength Aluminum Alloys of the 7000 Series

The development of the crack resistance curves requires that the crack resistance of the material be determined as a function of the crack extension. It is recognized that the extent of slow crack extension may be a function of the initial half crack length, a_o. To study this effect, 20-in. wide panels were machined from 0.063 in. thick 7075-T6 aluminum alloy. Initial crack lengths, $2a_o$, equal to 2 in., 5 in., and 8 in., were tested. These results are shown graphically in Figure 8. It will be observed that the longer initial crack length resulted in greater slow crack extension. However, the $\mathcal{G}_c$ value (as given by the termination of the R curve) for this material, as determined from these tests, is essentially constant.

In modern fracture mechanics it is customary to allow for the stress relaxing effect of the zone of plasticity at the crack tip by adding a small increment to the measured crack length.[4] The increment added to the measured crack length is the radius of the plastic zone and is given in Equation 9 for plane stress conditions:

$$r_{ys} = \frac{E \mathcal{G}}{2\pi \sigma_{ys}^2} \tag{9}$$

The influence of the plastic zone on the crack resistance is shown as the dotted curve in Figure 8. The difference between the dotted and solid curves is small, but still significant.

In Figure 9, the derivatives of the crack resistance curves of these 7075-T6 aluminum alloy specimens are plotted against the half crack length. Also, the derivative of the driving force curve is plotted against the half crack length. The point of intersection of these two curves gives the value of half crack length at instability. The steep slope of the driving force curve for short values of the crack length accounts for the very small slow crack extension observed for the shorter values of initial crack length. Similar behavior has been reported by Brown[8] for data obtained using 24-in. wide panels of 2219-T86 aluminum alloy, which exhibited considerable stable slow crack growth. These data were reported in the Fifth Committee Report of the ASTM Fracture Test Committee.[9]

The crack resistance curves for 7075-T6 aluminum alloy are shown in Figure 10. The half crack length at instability for these specimens was determined by the intersection of the derivatives of the crack resistance and driving force curves using the techniques shown in Figure 9. Two methods were used for calculating $\mathcal{G}_c$. The first procedure involves substituting the value of "a" at instability into Equation 6. However, this procedure does not correct for the zone of plasticity at the tip of the crack. The second procedure involves the same determination of "a" at instability and determining $\mathcal{G}_c$ from the crack resistance curve. It will be observed that the crack resistance curves rise sharply to the point of crack initiation instability or the plane strain fracture toughness ($\mathcal{G}_{Ic}$). This point was detected by the "pop-in" technique as described by Boyle, Sullivan, and Krafft.[10] In the wide panel tests, small electrical resistance strain gages cemented to the specimen just ahead of the crack were used to detect the "pop-in."

The crack resistance curves continue to rise rather steeply with crack extension until instability is reached. These crack resistance curves show essentially the same shape regardless of the specimen width or thickness, except for deviations in the 20-in. wide panels, as instability is approached. Comparison of the solid curves (calculated with plastic zone correction) with the dotted curves (without plastic zone correction) shows very little difference, therefore the curves calculated with the plastic zone correction will be reported for this family of alloys.

The critical value of $\mathcal{G}$ increases as the specimen thickness decreases. This behavior would be anticipated since the size of the plastic zone relative to plate thickness increases as the plate thickness is reduced. The critical value of $\mathcal{G}$ as determined by both panel widths is essentially the same. This indicates that the 4-in. wide panel is sufficiently large for this material.

The crack resistance curves of 7079-T6 aluminum alloy are shown in Figure 11. It will be observed that the $\mathcal{G}_c$ values determined, using the 4-in. wide specimen, were depressed when compared with the values determined from the 20-in. wide specimen. Examination of the detailed experimental data in Table III shows that the σ_{net}/σ_{ys} ratio for the 4-in. wide specimens approached unity. Under these conditions, the $\mathcal{G}_c$ value may be depressed.

The crack resistance curves for 7178-T6 aluminum alloy are shown in Figure 12. The crack resistance curves for the 4-in. wide panels show the same behavior as that exhibited by the 7075-T6 aluminum alloy. This behavior is considered normal. However, the behavior exhibited by the 20-in. wide panels is anomalous with the 1/4 in. thick panel showing the highest value of $\mathcal{G}_c$. Since this behavior is not in accord with expectations, an explanation is required to resolve this problem.

Since $\mathcal{G}_c$ is a measure of the energy required for crack propagation, an additional means of energy dissipation would have to be found for the 1/4 in. thick specimen if our expectations were correct. Most high strength aluminum alloys are characterized by weakness in the short transverse direction. In the example of the 7178-T6 aluminum alloy, the 1/4 in. thick specimen had sufficient elastic constraint to maintain essentially plane strain conditions. Under plane strain conditions, $\epsilon_z = 0$, so that a triaxial stress condition exists at the crack tip. This may lead to the opening of internal splits in the specimen. To determine if this is true, metallographic specimens were taken perpendicular to the path of crack propagation.

The profile of this fracture is shown in Figure 13. Numerous internal splits will be observed in the low magnification photomicrographs. Each internal split serves as a small thin specimen with accompanying plastic deformation. This disproportionately greater plastic deformation for this plate thickness will cause a higher value of $\mathcal{G}_c$. The high magnification photograph of this figure shows that these splits are associated with the grain boundaries or insoluable second phase particles.

If these ideas are correct, then the lower $\mathcal{G}_c$ values associated with the 1/8 in. and 1/16 in. thick sheets will be associated with a reduction in the number of internal splits. Metallographic studies of the 1/8 in. and 1/16 in. thick specimens are shown in Figures 14 and 15, respectively. It will be observed that the number of internal splits decreases as plane stress conditions are approached. The profile of the 1/16 in. thick specimen (Figure 15) is essentially free of internal splits.

The fracture toughness data for these alloys are summarized in Table III. Examination of these data shows that the ratio of σ_{net}/σ_{ys} was less than 0.80 for all the 20-in. wide panels tested. Consequently, the $\mathcal{G}_c$ values reported have not been influenced by yielding on the net section. The Fifth Committee Report[9] of the ASTM Fracture Test Committee shows that high nominal stresses may depress the $\mathcal{G}_c$ values so determined to a greater extent than anticipated from an analysis of the $\mathcal{G}$ and R curves. In the example of the lower toughness-higher strength alloys, 7075-T6 and 7178-T6, the correction for the plastic strain zone at the crack tip did not appreciably alter the values of $\mathcal{G}_c$ obtained. Further examination of these data shows a small but significant effect of specimen width on the $\mathcal{G}_c$ value does exist. Since some doubt has been raised concerning the general application of the tangent equation, the $\mathcal{G}_c$ values for 7075-T6, 7079-T6, and 7178-T6 were computed using the relationships developed by Isida.[11] These calculations resulted in an over-all elevation of the $\mathcal{G}_c$ values, but failed to eliminate the geometric size effect. Further studies are needed to establish this behavior fully.

Since the primary objective here is to develop and illustrate principles, the simpler tangent equation was used for all calculations.

The 4-in. wide specimens of 7079-T6 were too small, as evidenced by a σ_{net}/σ_{ys} ratio greater than 0.80. Also, it will be noted that the $\mathcal{G}_c$ value was depressed when compared to the value determined using the 20-in. wide specimen.

High Strength Aluminum Alloys of the 2000 Series

The alloys studied in this phase of the investigation include 2014-T6, 2024-T4, and 2219-T81. The crack resistance curves for the 2014-T6 aluminum alloy are shown in Figure 16. It will be observed that the crack resistance curves developed using the 4-in. wide specimen gave significantly lower values of $\mathcal{G}_c$ than those determined

using the 20-in. wide specimens. Examination of the detailed experimental data for the 4-in. wide specimens showed that the net section stress at instability was slightly greater than the yield strength (Table IV).

To study the effect of high net section stress at failure, 20-in. wide panel specimens were machined from the 1/8 in. thick 2014-T6 aluminum alloy. Initial slot lengths of 0.50 in., 1.00 in., and 1.50 in. were tested. The crack resistance curves developed from this series of tests are shown in Figure 17. The dotted curve is a plot of the ASTM Fracture Test Committee's(9) recommended limit of applicability, namely, the net section stress should not exceed 0.8 times the yield strength.

It will be observed that the crack resistance curves determined using the three short crack lengths extend beyond the limit of applicability, as shown by the dotted line. The $\mathcal{G}_c$ values determined under these conditions are depressed when compared with the values determined using a specimen having an 8 in. long crack with low net section stress. The crack resistance curve developed using a specimen having an 8 in. long crack falls within the limit of applicability. Examination of the detailed experimental data for this specimen showed that the ratio of net section stress to yield strength was less than 0.80.

The usually high value of $\mathcal{G}_c$ determined from the 1/4 in. thick specimen of 2014-T6 aluminum alloy (Figure 16) is considered anomalous. Detailed examination of the specimen gave no clue as to the cause of this high value. Apparently some variable in the processing history of this sheet has resulted in the high value of fracture toughness. However, this behavior has been observed previously, on occasions, with other materials.

In attempting to analyze instability conditions for the lower strength-higher toughness materials (as exemplified by 2024-T4, 2219-T81, and 5456-H343 aluminum alloys), it must be realized that the plastic strain zone at the crack tip is not small compared to the crack length. Consequently, the derivative of the driving force curve should account for the effect of the plastic zone size. The expression which was used is given in Equation 10:(12)

$$\frac{d\mathcal{G}}{da}\left(\frac{W}{\mathcal{G}}\right) = \frac{2\pi}{\sin\frac{2\pi}{W}(a+r_{ys}) - \frac{2\pi r_{ys}}{W}} \qquad (10)$$

The value of r_{ys} is defined by Equation 9. The $\mathcal{G}_c$ values calculated using the crack length determined by Equation 10 were compared with the values of $\mathcal{G}_c$ calculated using the crack length determined from Equation 6. This was done for the three thicknesses of 2024-T4 aluminum alloy and the 0.125 in. thick specimen of 7075-T6 aluminum alloy. Use of Equation 10 resulted in an average change of only 11 percent in $\mathcal{G}_c$ for the 2024-T4 aluminum alloy and no change in $\mathcal{G}_c$ for the 7075-T6 aluminum alloy. Therefore, Equation 6 was used to compute the instability conditions for all the materials.

The instability conditions of 2024-T4 aluminum alloy are shown in Figure 18. The degree of success in defining the instability conditions for this material, using linear elastic fracture mechanics, is quite surprising. The mathematical equations call for essentially elastic behavior, that the zone of plasticity at the crack tip be small in comparison to the crack length, and that the net section stress be equal to or less than 0.80 of the yield strength. However, the difficulties encountered in making experimental measurements of this material due to its high fracture toughness and lower strength usually result in one or more of these conditions being violated. In spite of this, these instability curves appear reasonable.

The fracture resistance curves for this material are shown in Figure 19. In this figure the crack resistance curves developed with and without the plastic zone correction are presented. However, since the net section stress at instability exceeded 0.80 of the yield strength, it should be realized that the $\mathcal{G}_c$ value is depressed. Since wide panel data for this material are very limited, these values are presented for information.

The crack resistance curves for the 2219-T81 aluminum alloy are shown in Figure 20. Essentially the same remarks may be made concerning this material as were made for the 2024-T4 aluminum alloy.

The fracture toughness data for the 2000 series of aluminum alloys are summarized in Table IV. Except for the 20-in. wide panels of 2014-T6, all the net section stress to yield strength ratios exceed 0.80. Therefore, the $\mathcal{G}_c$ values reported are considered lower bound values. However, Tiffany(9) has reported fracture toughness values for 0.100 in. thick 2219-T87 aluminum alloy having a yield strength of 59,000 psi. His value for $\mathcal{G}_c$ of 1630 in. lb/in.^{2} with plastic zone size correction compares favorably with the value of 1525 in. lb/in.^{2} determined here for the 2219-T81 aluminum alloy. It is understood that his net section stress at failure met the less than 0.80 yield strength requirement.

It will be observed that the correction for the plastic zone size at the crack tip raises the $\mathscr{G}_c$ value for the lower strength materials by a factor of approximately 1.5. Such a large correction implies that the plastic zone size is not small compared to the crack length.

Strain Hardening Aluminum Alloy 5456-H343

The crack resistance curve for 5456-H343 aluminum alloy is shown in Figure 21. Essentially the same comments may be made for these data as were made for the 2000 series of aluminum alloys. The data for this alloy are summarized in Table V.

EFFECTS OF ALLOY PURITY ON FRACTURE TOUGHNESS

After having developed the basic fracture toughness data for the commercial aluminum alloys, it is reasonable to investigate the possibility of increasing the fracture toughness without sacrificing the strength of the material. The most promising avenue of approach would be to reduce the impurity levels of the alloys to as low a value as possible. Special melts of high purity 7075 and 2024 aluminum alloys were made. These materials were rolled to 0.125 and 0.090 in. thick sheets. Both 20-in. and 4-in. wide panels were machined from the 7075-T6 alloy, while only 20-in. wide panels were machined from the 2024-T4 alloy. The crack resistance curves developed for the high purity 7075-T6 alloy are shown and are compared with those for the commercial 7075-T6 alloy in Figure 22. The reduction of the impurity levels in this alloy has resulted in a significant increase in the fracture toughness. This is borne out by tests of both the 4-in. and 20-in. wide panels. Examination of these curves shows that instability was reached in the high purity alloy with less stable crack growth than in the commercial alloy. Examination of the curves for the 4-in. wide panels shows that the anisotropy is no more pronounced in the high purity alloy than in the commercial alloy.

The crack resistance curves for both the commercial and high purity 2024-T4 aluminum alloy are shown in Figure 23. A trend toward higher $\mathscr{G}_c$ values for the high purity material is indicated by these data. However, in an exceedingly tough material such as 2024-T4, one would not anticipate as great an improvement as in a low toughness material such as 7075-T6 aluminum. Furthermore, the experimental difficulties encountered in measuring the fracture toughness

of this material make a quantitative assessment of the improvement due to high purity melting and alloying quite difficult. The data for these materials are summarized in Table VI.

It will be noted that σ_{net}/σ_{ys} ratios for the 4-in. wide panels of high purity 7075-T6 are in excess of 0.80 maximum. Therefore, the $\mathscr{G}_c$ values for this series of tests are depressed. However, the 20-in. wide panels give reliable fracture toughness values, and a quantitative evaluation of the effects of high purity may be made.

ENERGY ABSORBING MECHANISMS

The results of this study have shown that the high purity 7075-T6 and 2024-T4 aluminum alloys exhibited higher values of fracture toughness than the same commercial alloys. If some insight could be gained into the fine mechanisms responsible for this upgrading of fracture toughness, then it may be possible to exercise control over those metallurgical factors which govern this property. The plane stress fracture behavior which has been the major subject of this paper is extremely difficult to analyze. Therefore, attention will be focused on the plane strain fracture toughness for simplicity.

It has been shown that the $\mathscr{G}_{Ic}$ values for the high purity alloys are approximately 60 to 100 percent greater than those for the corresponding commercial alloy. These values represent the work required to cause unit crack propagation per unit thickness under plane strain conditions. The energy absorbed may be divided into two parts. The first part consists of the surface free energy and the second part, the energy of plastic deformation. However, in comparing similar or essentially the same materials, it is reasonable to assume that the surface free energy term is approximately the same and the differences are a result of the work of plastic deformation.

Krafft[13] and Beacham[14] have developed a model to describe the fracturing process. In this model, they have theorized that precracking occurs in advance of the crack front and that these precracks originate at particles or discontinuities in the metal matrix. The solid material between the precrack then acts as a small tensile specimen and ultimate failure is by microvoid coalescence. This mechanism of fracture results in the formation of ductile rupture dimples on the fracture surface as discussed by Crussard et al.[15]

If our initial assumption concerning the work of plastic deformation is correct, then this may be reflected in the volume of intensely deformed metal on the fracture surface. It is now possible to determine the volume of highly deformed metal in the ductile rupture dimples by means of quantitative electron microfractography.

The fracture surface was replicated using the two-stage plastic method. The replica, after stripping from the specimen, was coated with carbon and shadowed with carbon. Stereoscopic photomicrographs were taken by tilting the specimen holder containing the replica through an angle of 10 degrees. Typical photomicrographs of the dimpled structure observed in the high purity and commercial 2024-T4 aluminum alloy are shown in Figures 24 and 25, respectively. Superficial examination of these fractographs revealed no difference in the fracture appearance of these alloys.

However, by using the stereographic photomicrographs it is possible to determine the height of the dimples by means of the parallax difference, as illustrated in Figure 26. The height of the dimples is given by Equation 11:

$$d = \frac{\ell_2 h_1 - h_2 \ell_1}{\sqrt{\ell_2^2 + h_2^2}} \qquad (11)$$

The volume of plastically deformed metal was calculated from the diameter and height of the ductile rupture dimples. The results of these calculations are given in Table VII. Attention is directed to the following two facts: (1) the average diameter of the dimples in the high purity 2024-T4 alloy is slightly larger than the corresponding diameter in the commercial alloy, and (2) the volume of the dimples is approximately ten times greater in the high purity alloy than in the commercial alloy. According to the Krafft-Beacham model, this implies a greater volume of metal subjected to intense plastic deformation. Similarly it may be possible to relate the difference in the volume of intensely deformed metal to the structure of the alloy. However, this volume is only one-ten thousandth of the total volume of metal subjected to plastic deformation in the fracture process (see Table VII).

Metallographic specimens from the fracture specimen were cut parallel to the path of crack propagation. Examination parallel to path of crack propagation showed that the high purity material has a more irregular and jagged appearance, normally indicative of higher

energy absorption (Figure 27). Further metallographic examination revealed that the only essential difference between the two alloys was in the degree of homogeneity (Figure 28). The commercial 2024-T4 alloy shows a much higher percentage of undissolved second phase particles than the high purity material. Gurland and Plateau(16) have shown that precracking may occur at these particles. Consequently, the distribution of these particles and the local ductility of the matrix adjacent to these particles will be the parameters influencing the volume of the ductile rupture dimples. Electron microprobe studies were made of both alloys. Both the high purity and commercial alloys have copper rich particles. There is a uniform distribution of copper in the matrix. In the commercial alloy, iron and manganese are associated with the particles while the silicon is uniformly distributed in the matrix. The high purity alloy was essentially free of iron and silicon. Therefore, the high purity alloy would have larger, and possibly more widely spaced, dimples, as the data show.

Similar results were obtained for the high purity and commercial 7075-T6 aluminum alloys. These confirm earlier observations by Carman, Armiento and Markus.(17)

It is possible now by analogy to extend the fractographic analysis discussed for the plane strain conditions to plane stress conditions. With the high purity material, the precracking is spaced further apart so that the extent of intense plastic deformation is greater and, thus, results in greater fracture toughness.

It is acknowledged that the ideas expressed in this section are somewhat speculative and certainly do not consider all the events which may occur in the plastic zone. However, it is felt that an extension of these observations and ideas may help to relate the macroscopic behavior and the micro mechanisms of fracture which have been the subject of metallurgical research for many years.

CONCLUSIONS

1. The fracture toughness of both commercial and high purity aluminum alloys of the 7000 and 2000 series has been determined by means of the center notched sheet specimen.

2. The instability conditions described here give reproducible and well defined values of fracture toughness.

3. For the very high strength aluminum alloys, the 4-in. wide specimen is sufficiently large to give accurate values of fracture toughness.

4. Both the compliance and photographic method give the same value of fracture toughness, provided the proper experimental conditions are met.

5. The testing conditions for the 2000 series of aluminum alloys do not conform to the normal requirements for simple fracture mechanics analysis, but the data may be analyzed within the framework of a refined instability model.

6. The fracture toughness of the 2000 series of aluminum alloys is greater than the fracture toughness of the 7000 series of aluminum alloys.

7. Reduction of iron and silicon contents results in an upgrading of the fracture toughness for both 7075-T6 and 2024-T4 aluminum alloys.

8. Quantitative fractography gives some insight into the mechanisms which may be responsible for the upgrading of the fracture toughness.

ACKNOWLEDGMENTS

The authors wish to thank Dr. Paul C. Paris, of Lehigh University, and Dr. G. R. Irwin, of the U. S. Naval Research Laboratory, for their assistance during the investigation and their review of the final paper. The authors wish to acknowledge the assistance of Miss Marie Dougherty, of Frankford Arsenal, who conducted the mechanical tests and Mrs. Mary Schuler, of Frankford Arsenal, for her work with the electron microscope.

REFERENCES

1. G. R. Irwin and J. E. Srawley, "Progress in the Development of Crack Toughness Fracture Tests", Materialprufung, Vol. 4, No. 1, pp 1-11, Jan. 1962.

2. G. R. Irwin, "Relation of Crack Toughness Measurements to Practical Applications", Weld. J. Res. Suppl., Nov. 1962.

3. J. M. Krafft, A. M. Sullivan and R. W. Boyle, "Effect of Dimensions on Fast Fracture Instability of Notched Sheets", Symposium on Crack Propagation, The College of Aeronautics, Cranfield, England, Sept. 1961.

4. G. R. Irwin, "Fracture Testing of High Strength Sheet Materials Under Conditions Appropriate for Stress Analysis", Naval Research Laboratory Report No. 5486, July 1960.

5. J. E. Srawley and W. F. Brown, "Fracture Toughness Testing," NASA Technical Memorandum TMX-52030.

6. G. E. Normark, B. W. Lifka and J. G. Kaufman, "Fracture Toughness, Fatigue-Crack Propagation and Corrosion Characteristics of Aluminum Alloy Plates for Wing Skins", Aluminum Company of America Quarterly Report, June 3, 1964 to Sept. 3, 1964, Contracts AF33(167)-11155 and AF33(615)-2012.

7. R. W. Boyle, "A Method for Determining Crack Growth in Notch Specimens", Materials Research and Standards, ASTM, Aug. 1962.

8. W. F. Brown, "Comments on the K_c Data Used in the Fifth Committee Report", Notes for ASTM Committee Meeting.

9. "Progress in Measuring Fracture Toughness and Using Fracture Mechanics", Fifth Report of Special ASTM Committee on Fracture Testing of High Strength Materials, Materials Research and Standards, Vol. 4, No. 3, p 107, March 1964.

10. R. W. Boyle, A. M. Sullivan and J. M. Krafft, "Determination of Plane Strain Fracture Toughness with Sharply Notched Sheets", Weld. J. Res. Suppl. 428-s to 432-s, 1962.

11. M. Isida, "The Effect of Longitudinal Stiffeners in a Cracked Plate Under Tension", Proceedings, Fourth U. S. Congress of Applied Mechanics, 1962.

12. Private communication from G. R. Irwin.

13. J. M. Krafft, "Correlation of Plane Strain Crack Toughness with Strain Hardening Characteristics", Applied Materials Research, Dec. 1963.

14. C. D. Beacham, "An Electron Fractographic Study of the Influence of Plastic Strain Conditions Upon Ductile Rupture Processes in Metals", Trans. ASM, Vol. 56, No. 3.

15. D. Crussard, J. Plateau, R. Tamhankar, G. Henry and D. Lajeunesse, "A Comparison of Ductile and Fatigue Fracture", Fracture (Swampscott Conference, 1959), John Wiley and Sons, Inc., New York, 1959.

16. J. Gurland and J. Plateau, "The Mechanism of Ductile Rupture of Metals Containing Inclusions", Trans. ASM, Vol. 56, No. 3.

17. C. M. Carman, D. F. Armiento and H. Markus, "Plane Strain Fracture Toughness of High Strength Aluminum Alloys", ASME Paper No. 64-WA/Met 11.

TABLE I

Aluminum Alloys and Product Dimensions

Alloy	Sheet Thickness (in.)
7075-T6	0.063, 0.125 and 0.250
7075-T6 (Hi Purity)	0.090 and 0.125
7079-T6	0.125
7178-T6	0.063, 0.125 and 0.250
2014-T6	0.063, 0.125 and 0.250
2219-T81	0.125
5456-H343	0.125
2024-T4	0.063, 0.125 and 0.250
2024-T4 (Hi Purity)	0.090 and 0.125

TABLE II

Engineering Tensile Properties of the Aluminum Alloys

Material	Direction	Yield Strength 0.20% Offset (psi)	Tensile Strength (psi)	Elong. (%)
7075-T6 Comm Sheet 1/16"	Long	76,900	85,000	11.5
	Trans	74,500	84,800	10.1
7075-T6 Comm Sheet 1/8"	Long	75,800	82,700	13.9
	Trans	73,500	84,500	12.4
7075-T6 Comm Sheet 1/4"	Long	75,600	81,500	12.2
	Trans	74,100	84,100	10.5
7075-T6 Hi Purity Sheet 0.090	Long	73,200	79,700	12.9
	Trans	71,700	81,300	13.2
7075-T6 Hi Purity Sheet 1/8"	Long	76,300	82,800	13.0
	Trans	72,000	81,800	13.1
7079-T6 Comm Sheet 1/8"	Long	74,700	81,600	12.4
	Trans	72,700	83,500	11.3
7178-T6 Comm Sheet 1/16"	Long	82,000	89,300	12.2
	Trans	79,100	89,600	11.6
7178-T6 Comm Sheet 1/8"	Long	82,700	90,100	14.2
	Trans	78,900	91,400	12.3
7178-T6 Comm Sheet 1/4"	Long	87,500	90,900	11.7
	Trans	85,300	92,500	11.3

TABLE II (Continued)

2014-T6 Comm Sheet 1/16"	Long	64,000	71,300	9.4
	Trans	63,500	71,200	10.8
2014-T6 Comm Sheet 1/8"	Long	65,300	71,100	11.2
	Trans	62,800	71,300	11.6
2014-T6 Comm Sheet 1/4"	Long	64,700	70,200	13.7
	Trans	63,300	70,400	12.9
2219-T81 Comm Sheet 1/8"	Long	52,200	66,000	11.2
	Trans	50,700	66,200	11.6
2024-T4 Comm Sheet 1/16"	Long	51,300	71,700	19.9
	Trans	46,200	69,500	19.3
2024-T4 Comm Sheet 1/8"	Long	49,000	66,300	17.8
	Trans	43,900	65,200	20.0
2024-T4 Comm Sheet 1/4"	Long	52,800	70,100	16.3
	Trans	47,500	69,300	18.8
2024-T4 Hi Purity Sheet 0.090	Long	53,100	73,200	18.8
	Trans	47,000	71,100	22.5
2024-T4 Hi Purity Sheet 1/8"	Long	58,000	75,200	17.5
	Trans	49,900	71,200	21.1
5456-H343 Comm Sheet 1/8"	Long	42,900	56,200	9.9
	Trans	41,900	58,200	13.1

TABLE III

Fracture Toughness Values for the 7000 Series of Aluminum Alloys

Alloy	No. of Tests	Thickness (in.)	Width (in.)	Direction	Stress at Instability (psi)	Half Crack Length at Instability (in.)	$\mathscr{G}_c$ WOPZS (in.lb/in^2)	$\mathscr{G}_c$ WPZS (in.lb/in^2)	$\frac{\sigma_{net}}{\sigma_{ys}}$
7075-T6	1	0.063	20	Long	18,150	4.660	571	600	0.44
7075-T6	1	0.125	20	Long	17,100	4.400	465	490	0.40
7075-T6	1	0.250	20	Long	12,000	4.960	257	276	0.30
7075-T6	4	0.063	4	Long	37,900	0.909	--	650	0.67
7075-T6	4	0.063	4	Trans	39,200	0.810	--	510	0.87
7075-T6	4	0.125	4	Long	43,500	0.778	--	530	0.87
7075-T6	4	0.125	4	Trans	30,400	0.769	--	370	0.71
7079-T6	1	0.125	20	Long	23,200	5.000	1020	1185	0.62
7079-T6	4	0.125	4	Long	41,400	0.920	--	581	0.96
7079-T6	4	0.125	4	Trans	37,600	1.090	--	620	0.94
7178-T6	1	0.063	20	Long	13,500	4.480	297	320	0.30
7178-T6	1	0.125	20	Long	15,500	4.500	393	420	0.34
7178-T6	1	0.250	20	Long	15,300	4.820	433	480	0.34
7178-T6	4	0.063	4	Long	35,000	0.577	--	261	0.63
7178-T6	4	0.125	4	Long	33,900	0.713	--	321	0.67
7178-T6	4	0.250	4	Long	28,800	0.890	--	310	0.67
7178-T6	4	0.063	4	Trans	32,400	0.610	--	236	0.60
7178-T6	4	0.125	4	Trans	26,300	0.693	--	173	0.54
7178-T6	4	0.250	4	Trans	19,100	0.807	--	109	0.41

TABLE IV

Fracture Toughness Values for the 2000 Series of Aluminum Alloys

Alloy	No. of Tests	Thickness (in.)	Width (in.)	Direction	Stress at Instability (psi)	Half Crack Length at Instability (in.)	$\mathscr{G}_c$ WOPZS (in.lb/in^2)	$\mathscr{G}_c$ WPZS (in.lb/in^2)	$\frac{\sigma_{net}}{\sigma_{ys}}$
2014-T6	1	0.063	20	Long	19,400	5.250	786	850	0.72
2014-T6	1	0.125	20	Long	22,000	4.400	769	910	0.61
2014-T6	1	0.250	20	Long	25,800	5.580	1499	1920	0.87
2014-T6	1	0.125	20	Long	58,000	0.690	705	1130	0.95
2014-T6	1	0.125	20	Long	51,000	0.890	705	1032	0.86
2014-T6	1	0.125	20	Long	47,800	1.300	909	1275	0.84
2014-T6	4	0.063	4	Long	40,500	0.813	--	698	1.00
2014-T6	4	0.125	4	Long	39,900	0.799	--	639	0.98
2014-T6	4	0.250	4	Long	35,300	0.954	--	661	1.02
2014-T6	4	0.063	4	Trans	38,800	0.773	--	538	0.93
2014-T6	4	0.125	4	Trans	33,700	0.853	--	448	0.85
2014-T6	4	0.250	4	Trans	24,900	1.039	--	305	0.76
2024-T4	1	0.063	20	Long	27,900	4.830	1430	2540	1.05
2024-T4	1	0.125	20	Long	24,200	4.930	1100	1450	0.98
2024-T4	1	0.250	20	Long	23,800	5.000	1088	1450	0.91
2219-T81	1	0.125	20	Long	25,200	4.800	1147	1525	0.93

TABLE V

Fracture Toughness Values for 5456-H343 Aluminum Alloy

No. of Tests	Thickness (in.)	Width (in.)	Direction	Stress at Instability (psi)	Half Crack Length at Instability (in.)	$\mathscr{G}_c$ WOPZS (in.lb/in^2)	$\mathscr{G}_c$ WPZS (in.lb/in^2)	$\frac{\sigma_{net}}{\sigma_{ys}}$
1	0.125	20	Long	23,200	4.820	1020	1465	1.02

TABLE VI

Fracture Toughness Values for High Purity and Commercial 7075-T6 and 2024-T4 Aluminum Alloys

Alloy	No. of Tests	Thickness (in.)	Width (in.)	Direction	Stress at Instability (psi)	Half Crack Length at Instability (in.)	$\mathscr{G}_c$ WOPZS (in.lb/in^2)	$\mathscr{G}_c$ WPZS (in.lb/in^2)	$\frac{\sigma_{net}}{\sigma_{ys}}$
7075-T6									
Comm.	1	0.063	20	Long	18,150	4.660	571	600	0.44
" "	1	0.125	20	Long	17,100	4.400	465	490	0.40
7075-T6									
H.P.	1	0.090	20	Long	26,300	4.550	1160	1310	0.66
" "	1	0.125	20	Long	26,600	4.500	1163	1320	0.64
7075-T6									
Comm.	4	0.063	4	Long	35,100	0.520	--	510	0.50
" "	4	0.063	4	Trans	39,200	0.810	--	510	0.87
" "	4	0.125	4	Long	43,500	0.778	--	530	0.87
" "	4	0.125	4	Trans	30,400	0.769	--	370	0.71
7075-T6									
H.P.	4	0.090	4	Long	56,500	0.980	--	975	1.52
" "	4	0.090	4	Trans	52,800	0.850	--	710	1.25
" "	4	0.125	4	Long	58,900	0.880	--	858	1.42
" "	4	0.125	4	Trans	50,600	0.775	--	540	1.08
2024-T4									
Comm.	1	0.063	20	Long	27,900	4.830	1430	2540	1.05
" "	1	0.125	20	Long	24,200	4.930	1100	1450	0.98
2024-T4									
H.P.	1	0.090	20	Long	28,900	4.650	1430	2100	1.00
" "	1	0.125	20	Long	29,900	4.580	1510	2170	0.95

TABLE VII

Evaluation of Plasticity Factors Affecting Fracture Toughness

Material	Spec. No.	Weighted Average Dimple Dia. (in.)	Weighted Average Dimple Height (in.)	Vol. of Metal Subject to Intense Plastic Deformation ($in.^3$)	$\mathcal{G}$ Ic ($in.lb/in^2$)	r_{ys} (in.)	Vol. of Plastic Zone ($in.^3$)
2024-T4 Comm	1	3.249×10^{-6}	2.788×10^{-7}	2.974×10^{-7}	--	--	--
	2	3.300×10^{-6}	3.592×10^{-7}	2.806×10^{-7}	--	--	--
	3	4.672×10^{-6}	3.714×10^{-7}	2.904×10^{-7}	--	--	--
Average				2.895×10^{-7}	145	3.14×10^{-2}	3.07×10^{-3}
2024-T4 H.P.	1	4.028×10^{-6}	1.812×10^{-6}	29.38×10^{-7}	--	--	--
	2	4.199×10^{-6}	0.967×10^{-6}	10.60×10^{-7}	--	--	--
	3	6.947×10^{-6}	1.669×10^{-6}	21.60×10^{-7}	--	--	--
Average				20.53×10^{-7}	232	3.82×10^{-2}	4.59×10^{-3}

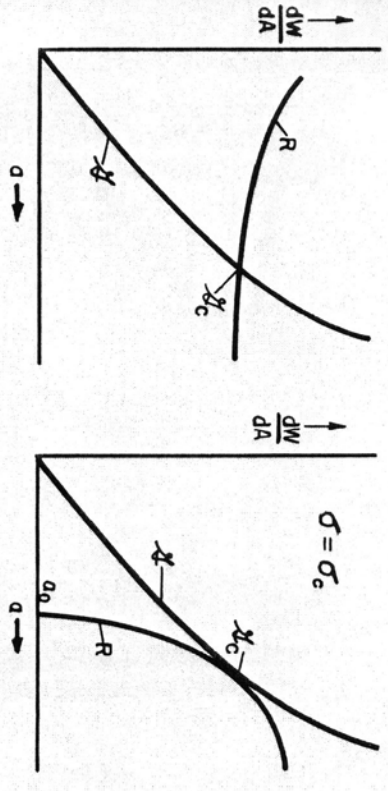

Figure 1. Schematic representation of crack instability.

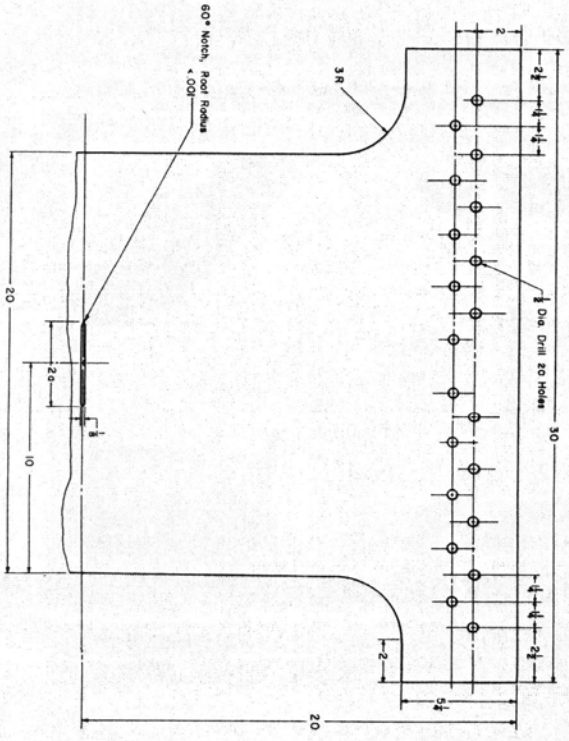

Figure 2. Twenty-inch wide panel specimen.

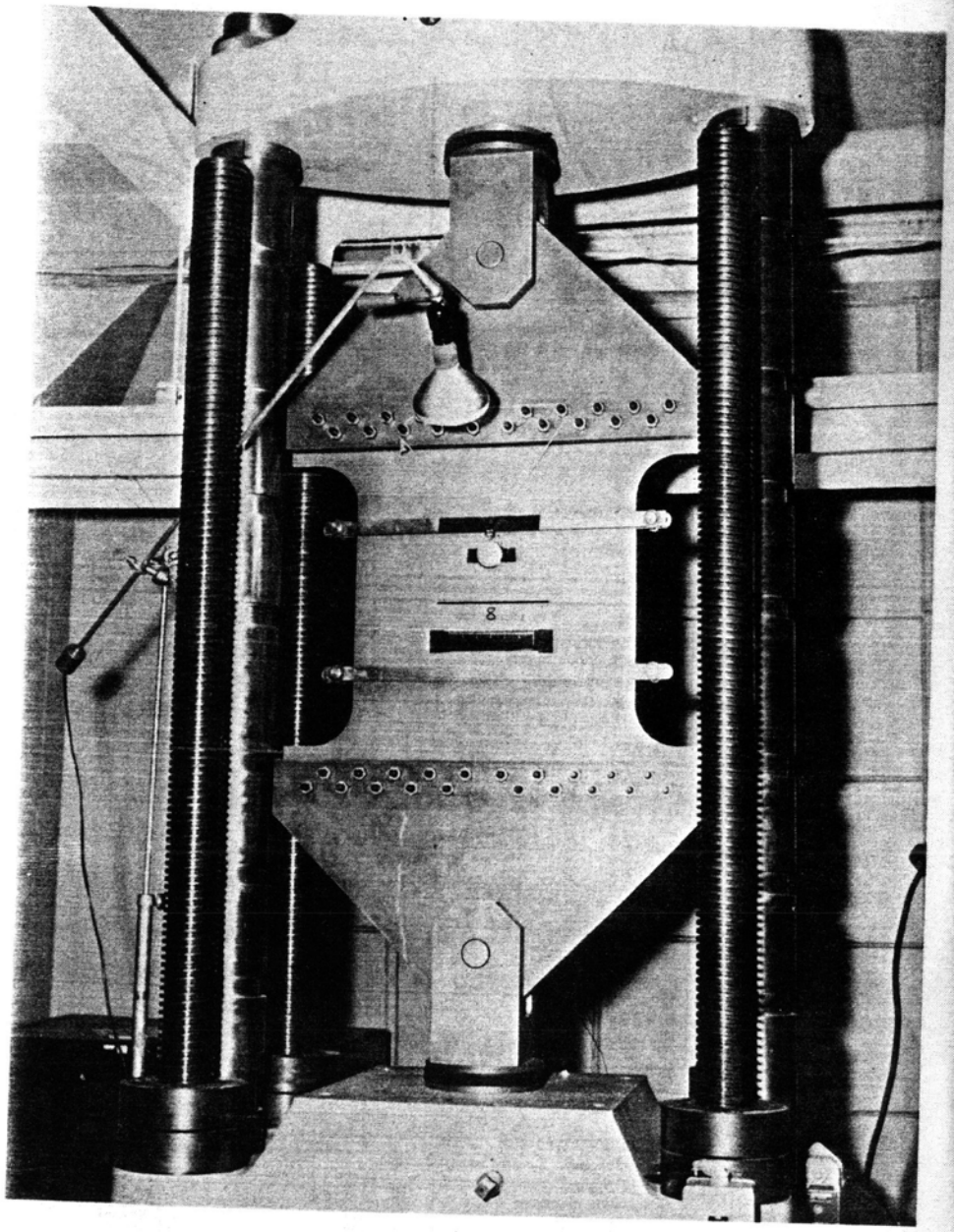

Figure 3. Assembled 20-in. wide panel specimen ready for test.

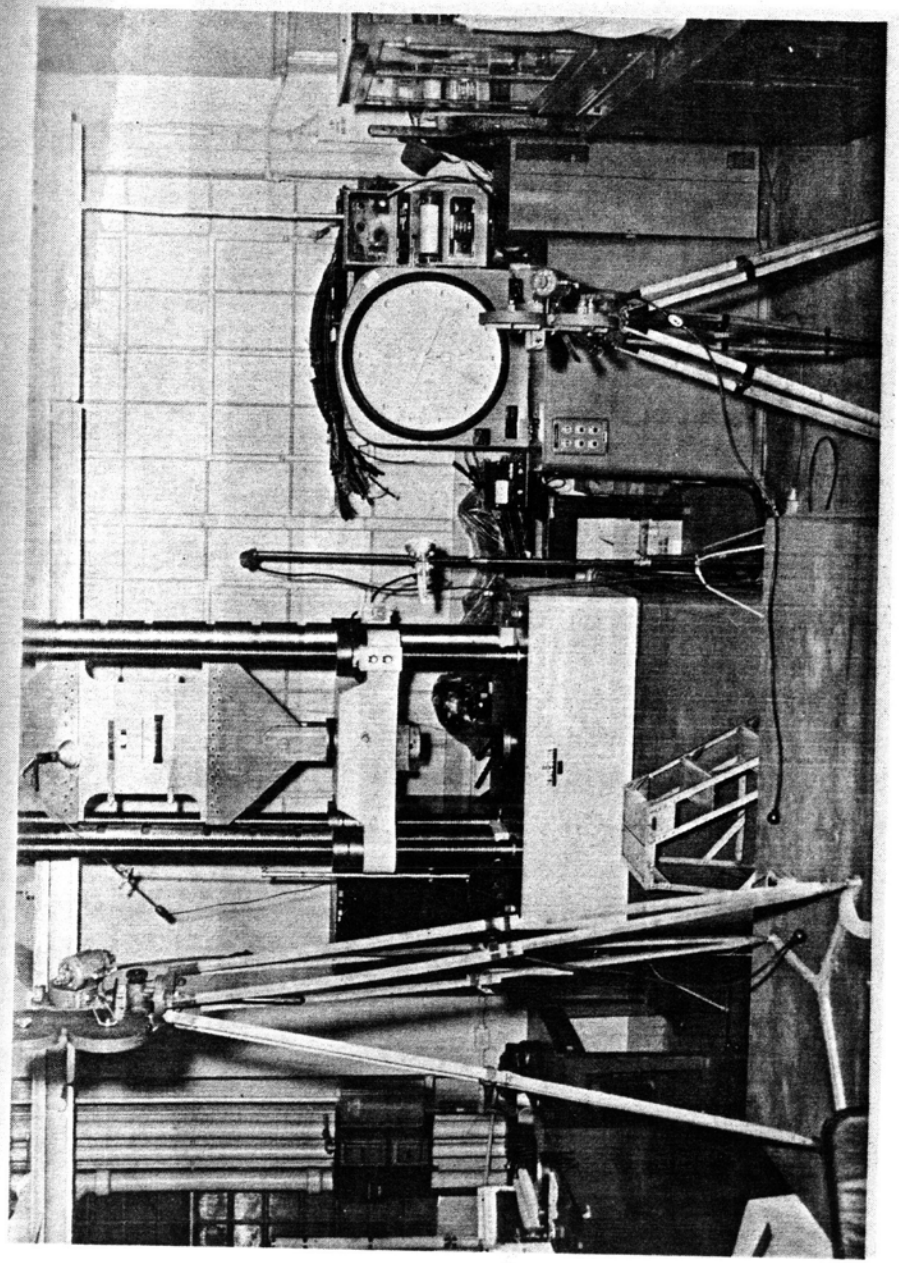

Figure 4. Experimental equipment used for photographic measurement of crack length and load.

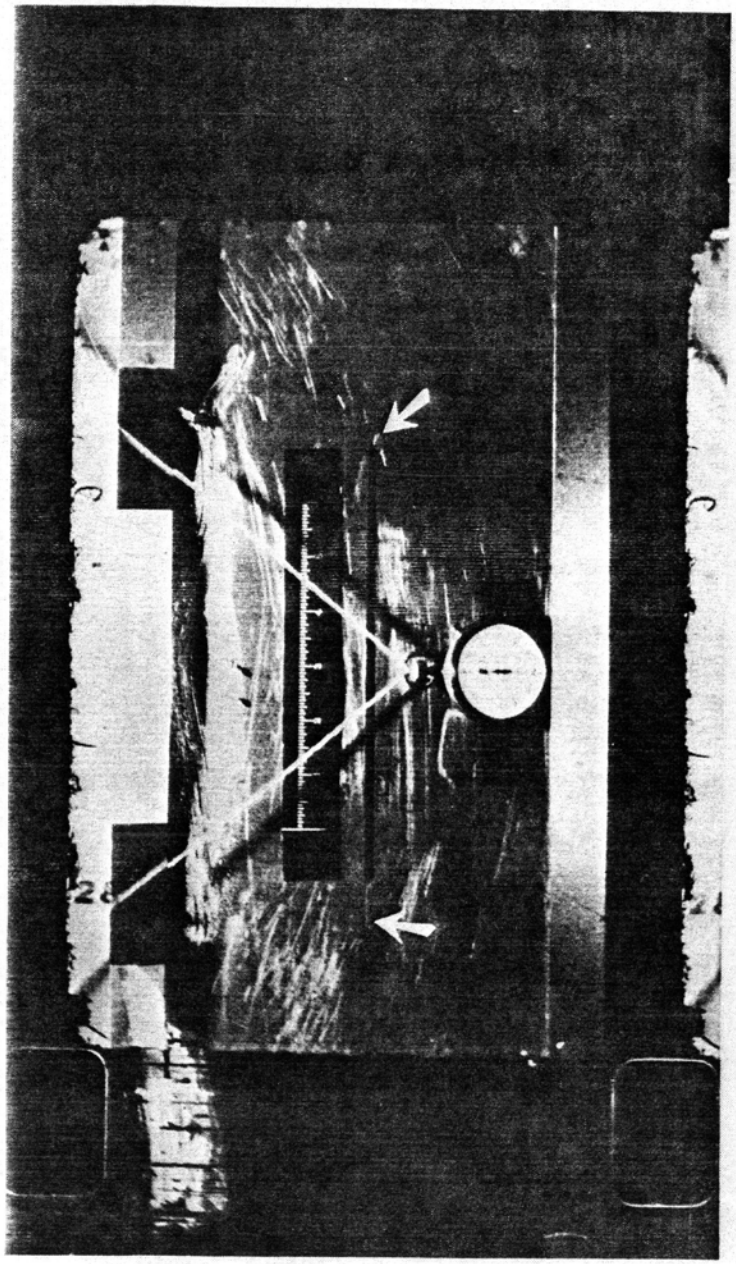

Figure 5. Photograph of crack just prior to instability in 1/8-inch thick 7075-T6 aluminum alloy. Photograph of the center 10 inches of the specimen.

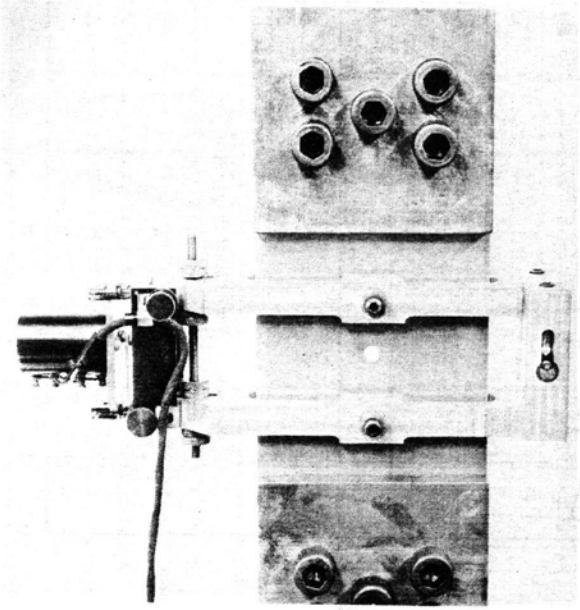

Figure 6. Displacement gage for 4-in. wide specimens.

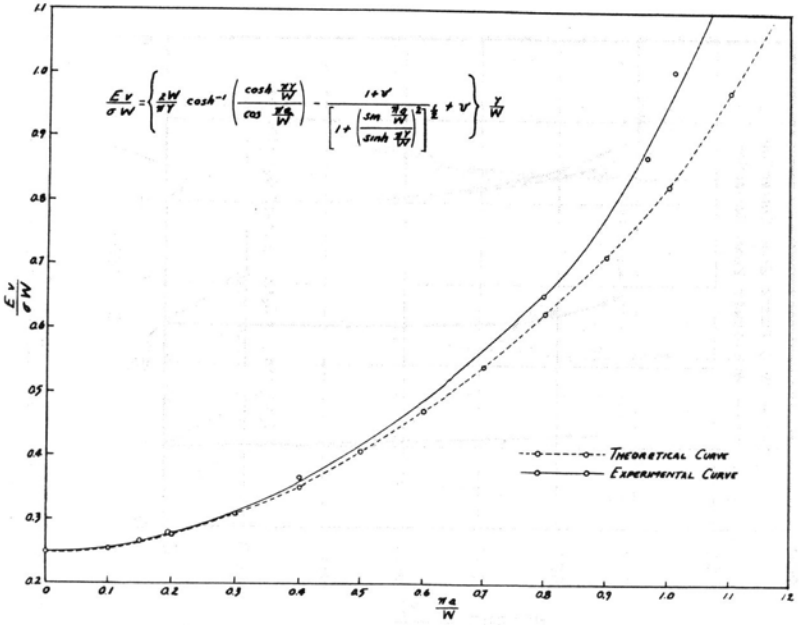

Figure 7. Calibration curves for displacement gage.

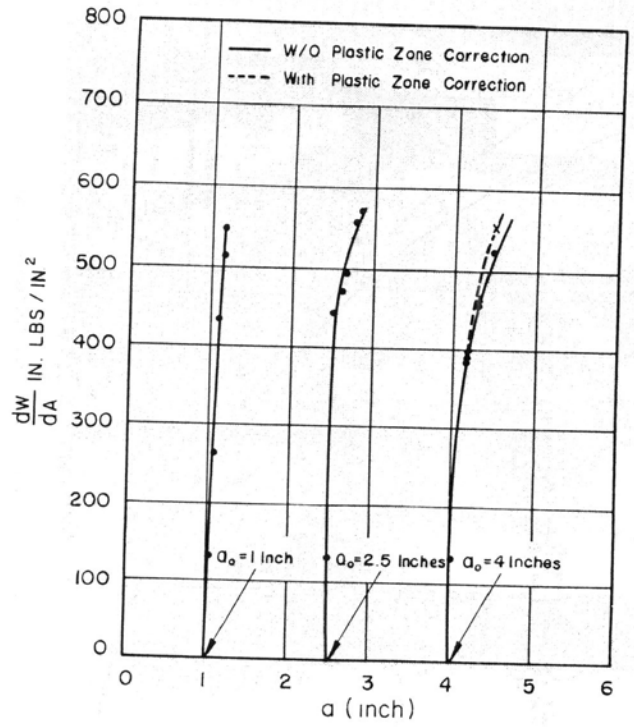

Figure 8. Crack resistance curves for 20 inch wide 1/16 inch thick 7075-T6 aluminum alloy as a function of initial crack length.

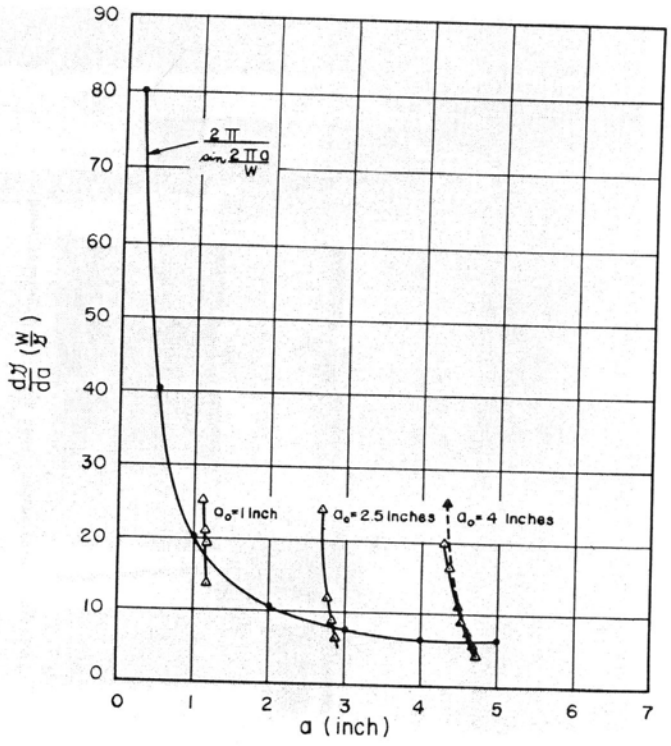

Figure 9. Instability analysis for 1/16-in. thick 7075-T6 aluminum alloy showing the effect of initial crack length on crack length at instability.

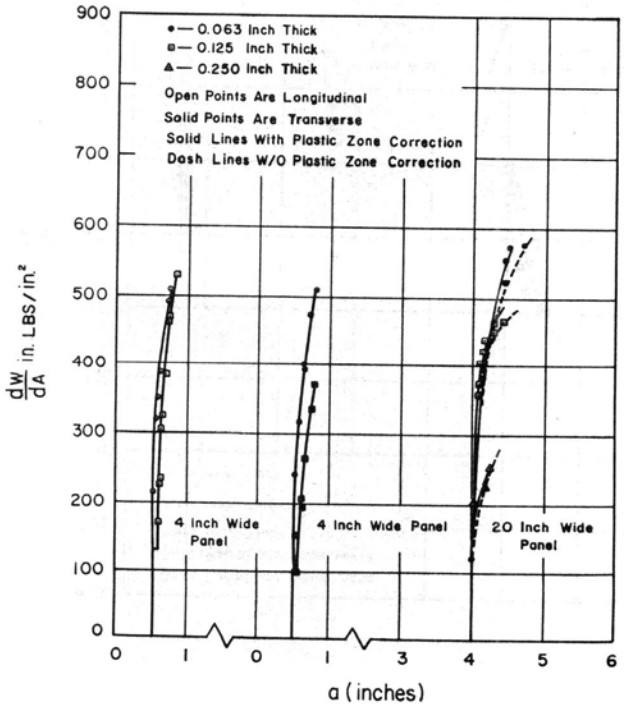

Figure 10. Crack resistance curves for 7075-T6 aluminum alloy.

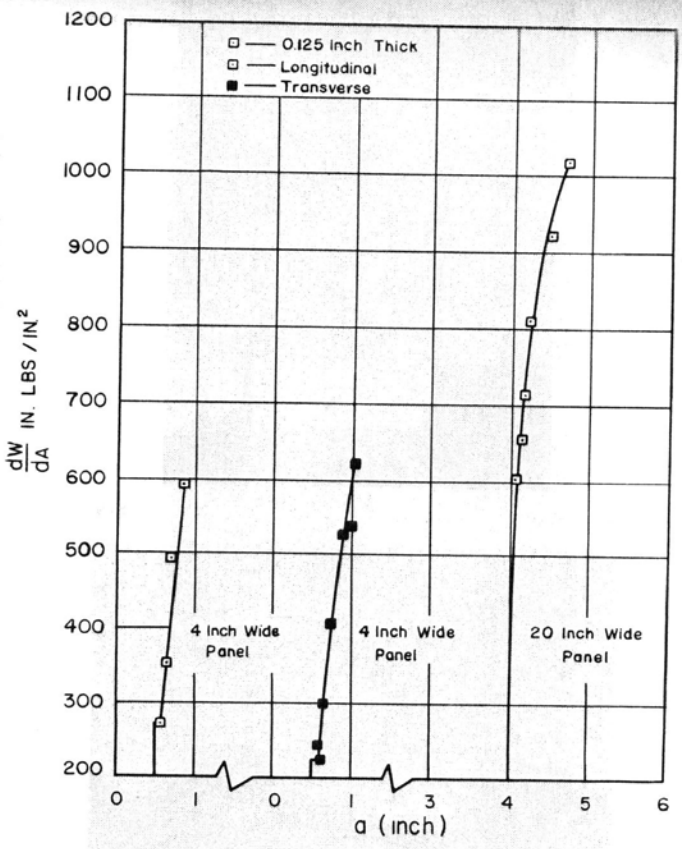

Figure 11. Crack resistance curves for 7079-T6 aluminum alloy.

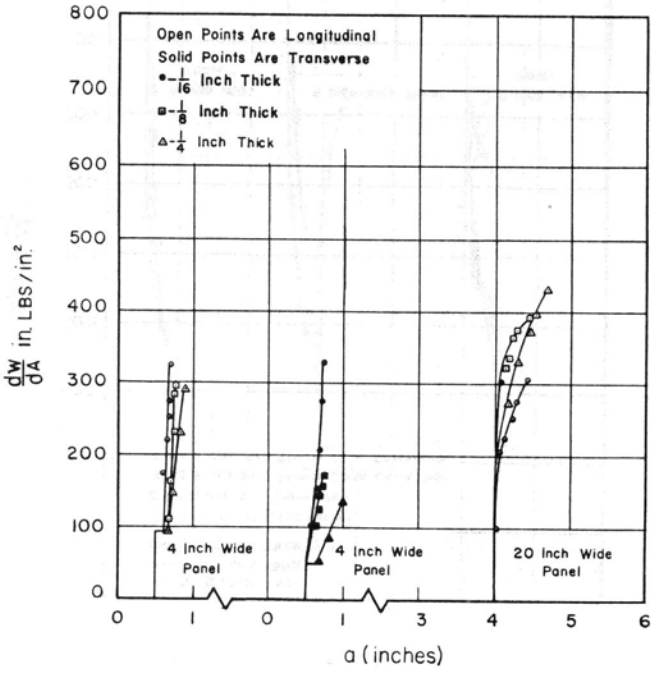

Figure 12. Crack resistance curves for 7178-T6 aluminum alloy.

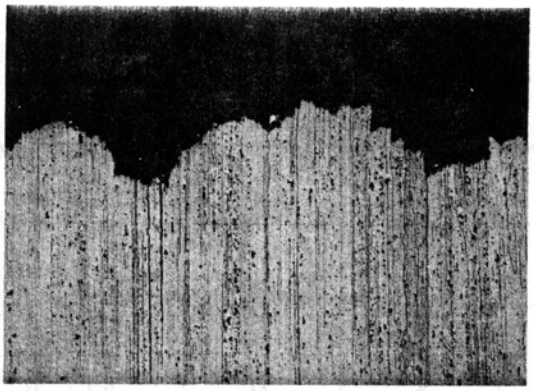

61X Kellers

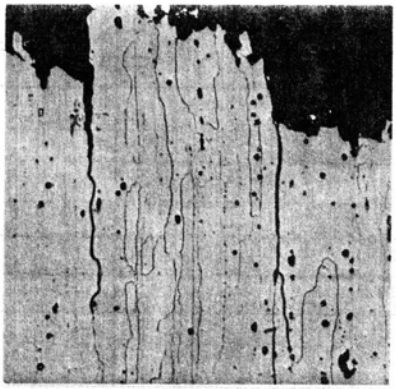

300X Kellers

Figure 13. Fracture profile of 1/4-in. thick 7178-T6 aluminum alloy specimen.

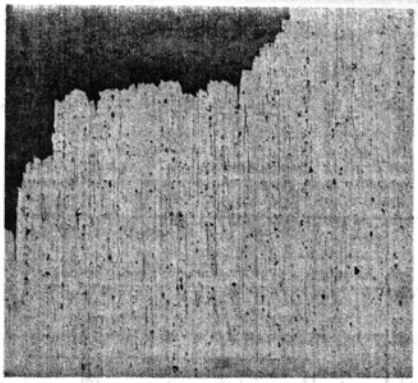

62X Kellers

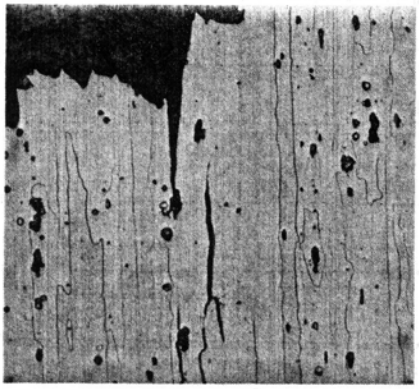

300X Kellers

Figure 14. Fracture profile of 1/8-in. thick 7178-T6 aluminum alloy specimen.

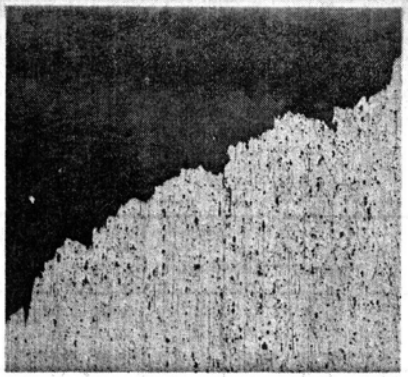

62X Kellers

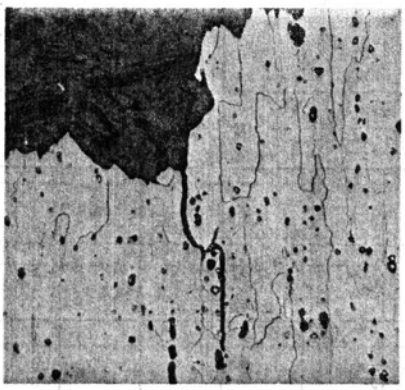

300X Kellers

Figure 15. Fracture profile of 1/16-in. thick 7178-T6 aluminum alloy specimen.

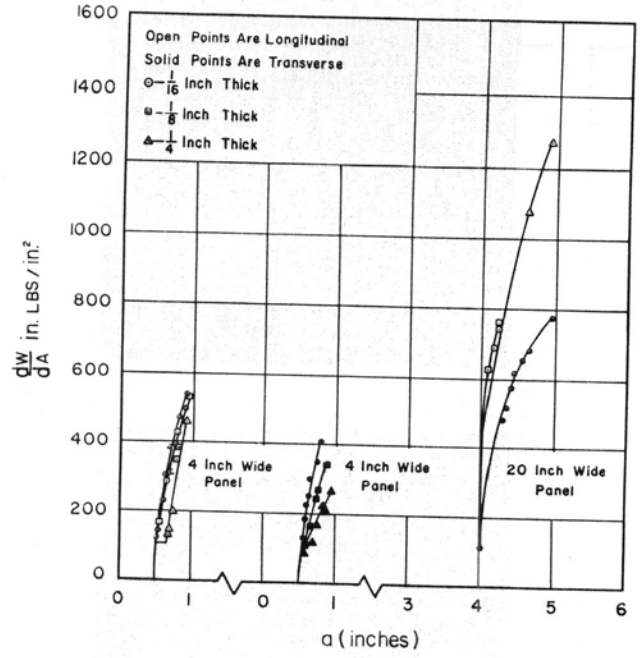

Figure 16. Crack Resistance curves for 2014-T6 aluminum alloy.

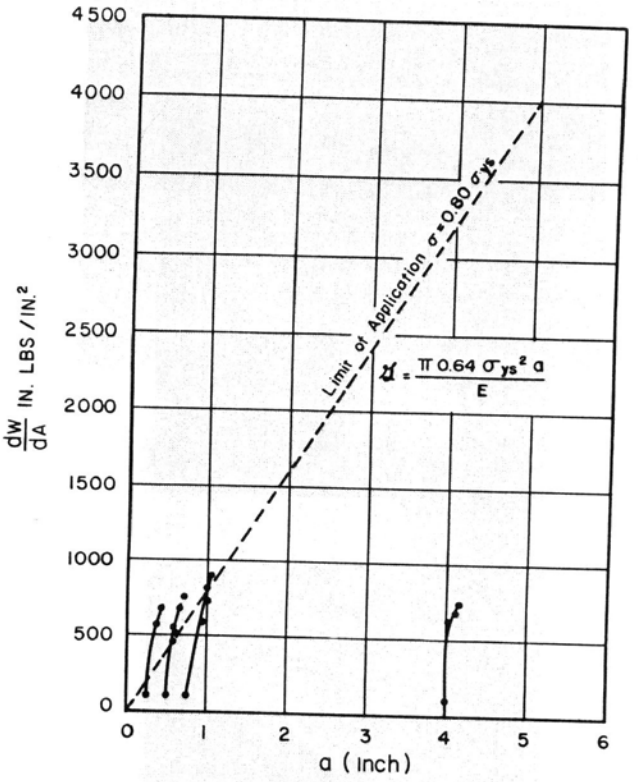

Figure 17. Crack resistance curves for 20 inch wide 1/8-inch thick 2014-T6 aluminum alloy showing effect of high stress on the Gc value.

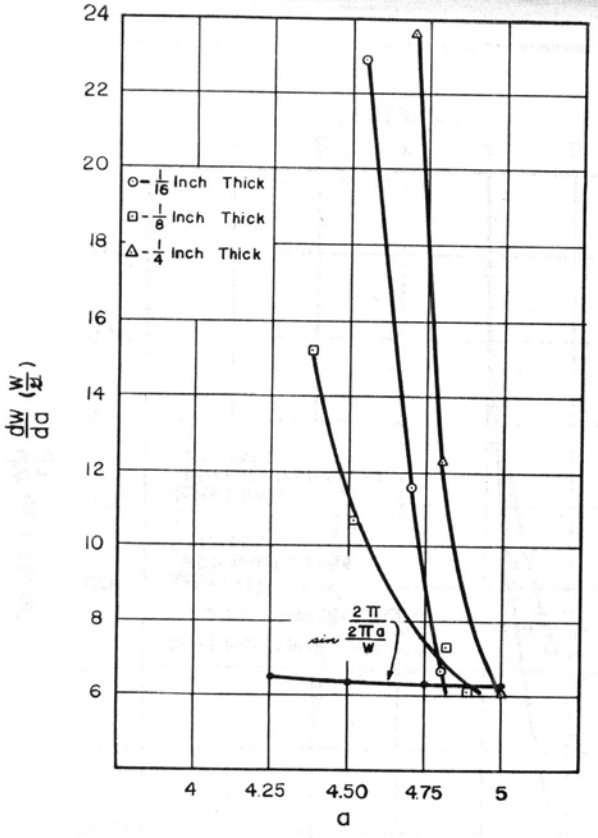

Figure 18. Instability analysis for 2024-T4 aluminum alloy.

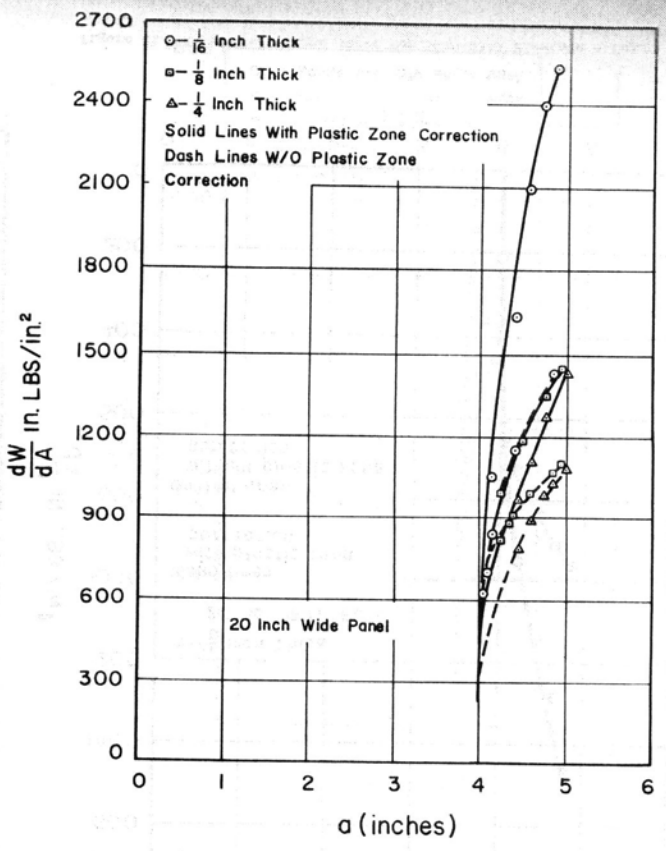

Figure 19. Crack resistance curves for 2024-T4 aluminum alloy.

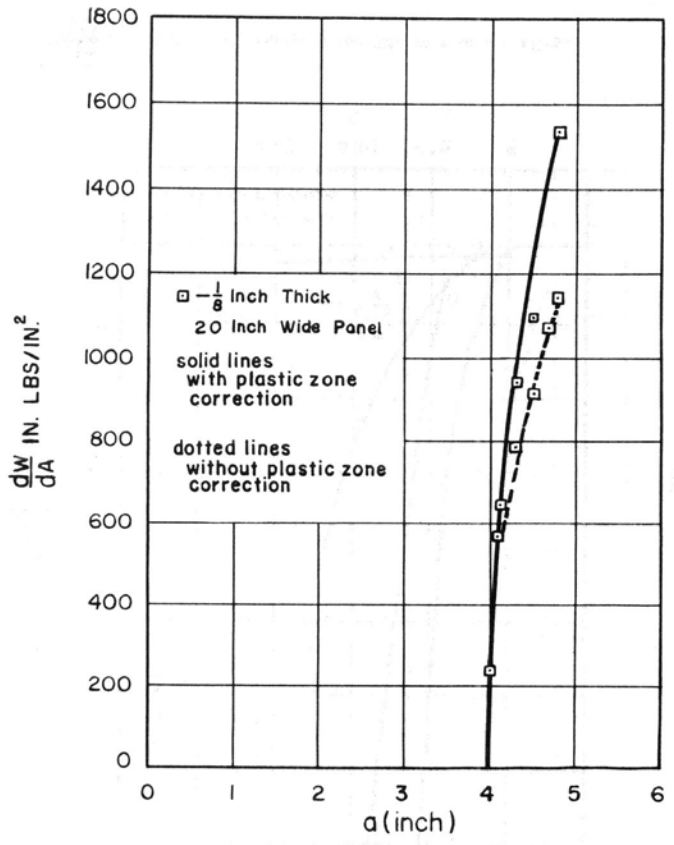

Figure 20. Crack resistance curve for 2219-T81 aluminum alloy.

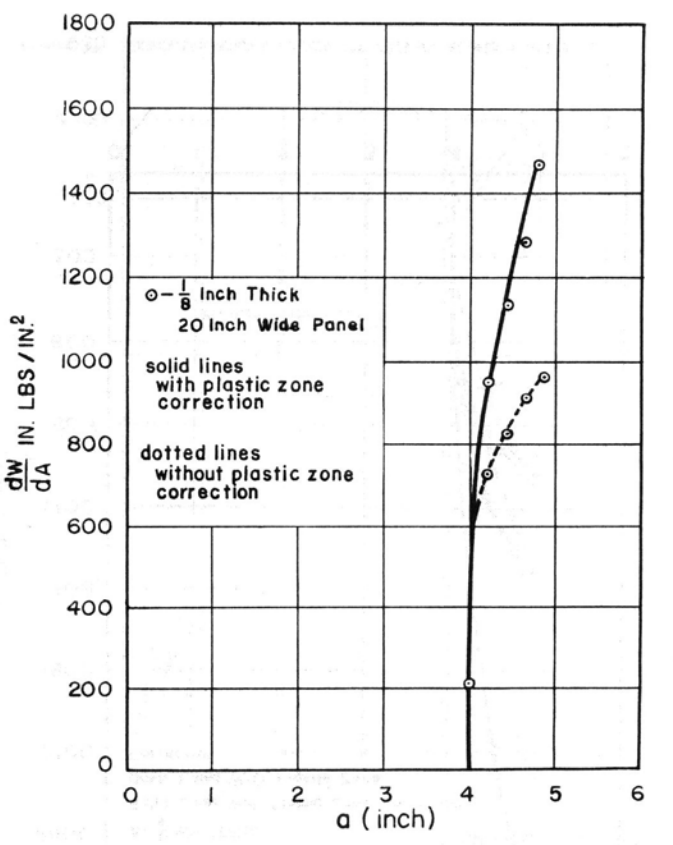

Figure 21. Crack resistance curve for 5456-H343 aluminum alloy.

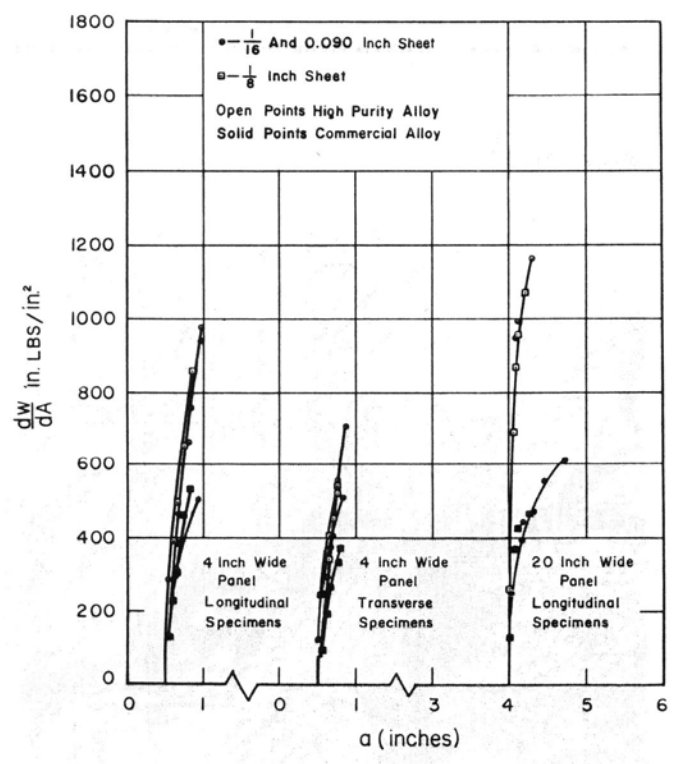

Figure 22. Comparison of the crack resistance curves for commercial and high purity 7075-T6 aluminum alloys.

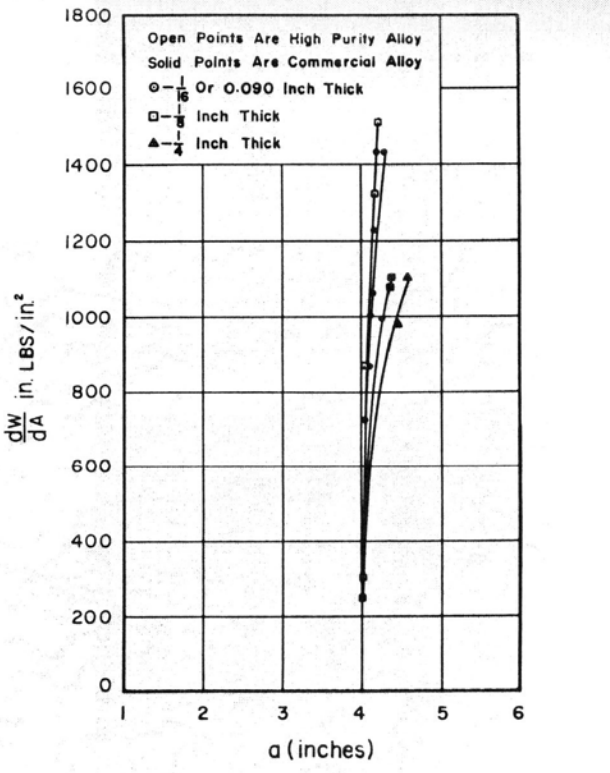

Figure 23. Comparison of the crack resistance curves for commercial and high purity 2024-T4 aluminum alloys.

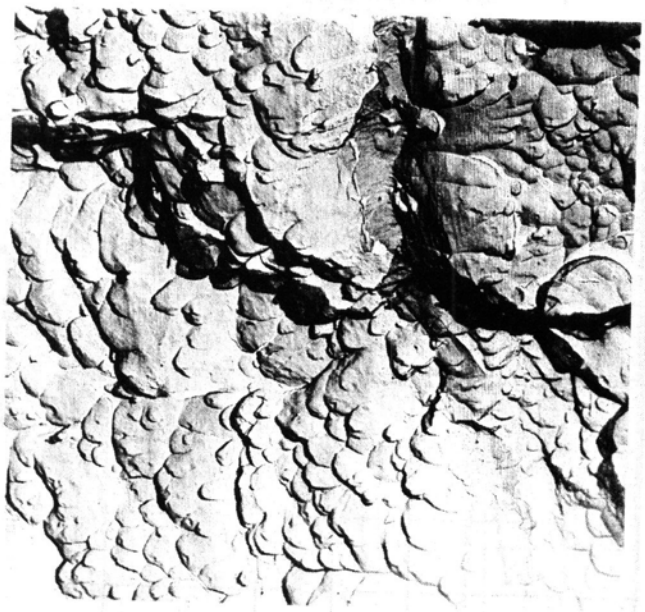

Mag 5500X

Figure 24. Fractograph showing dimple structure observed in commercial 2024-T4 aluminum alloy.

Mag 5400X

Figure 25. Fractograph showing dimple structure observed in high purity 2024-T4 aluminum alloy.

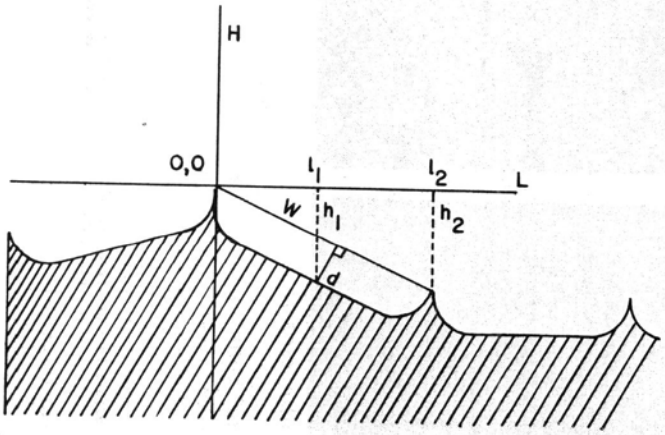

Figure 26. Sketch showing measurements needed to calculate the depth of the dimples.

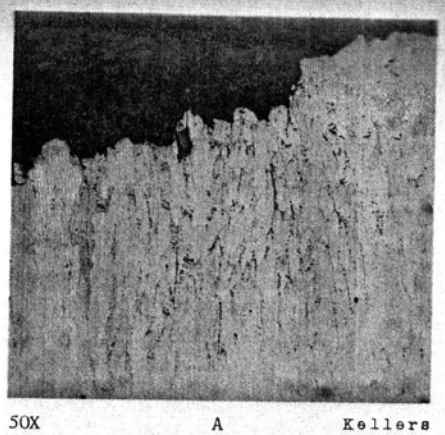

50X A Kellers

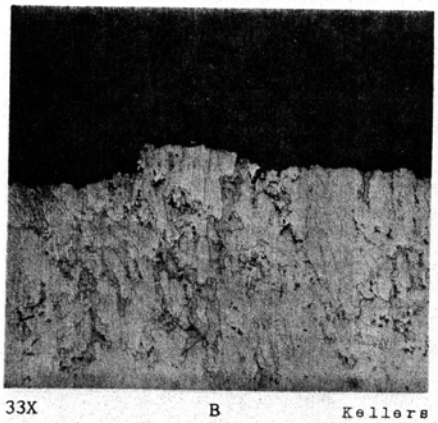

33X B Kellers

Figure 27. Fracture surfaces in 2024-T4 aluminum alloys.
A. High purity alloy B. Commercial alloy

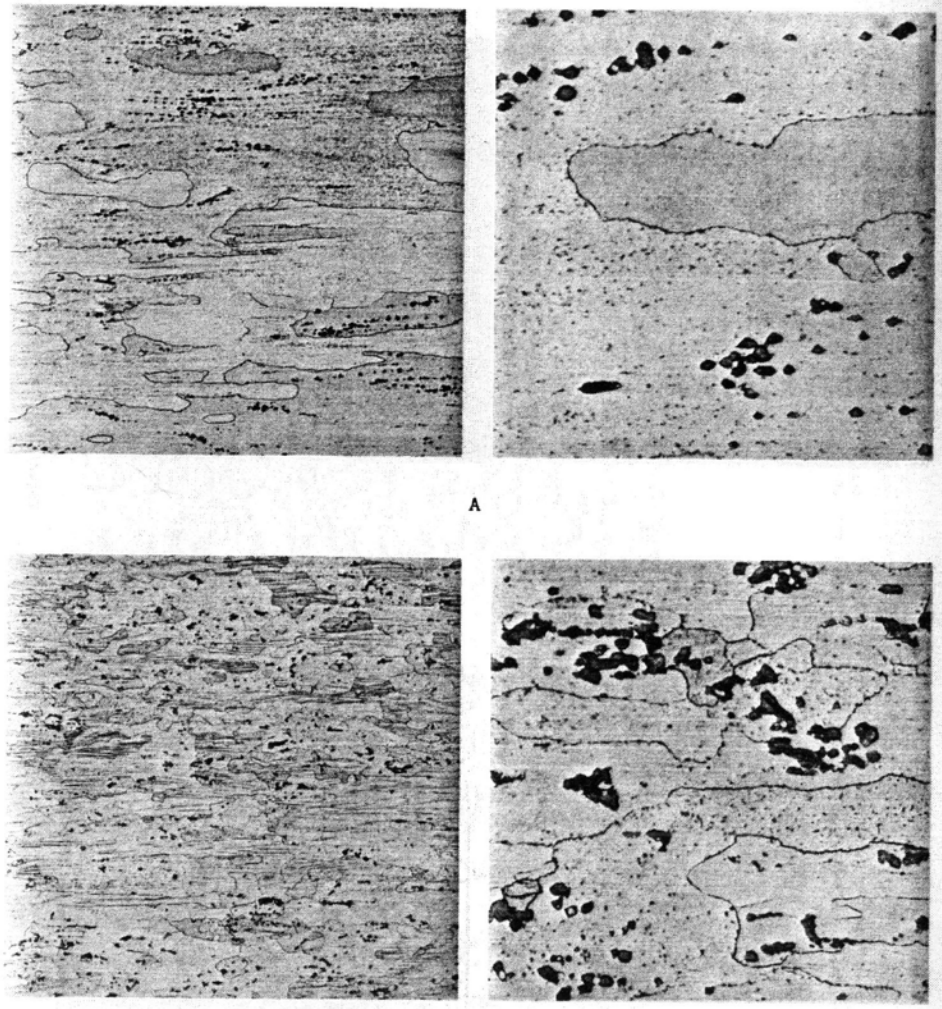

A

95X

470X

B

Figure 28. Structure of 2024-T4 aluminum alloys.
A. High purity alloy B. Commercial alloy

B III-5

TENSILE AND TORSIONAL FRACTURE OF LOW CARBON STEEL AT LIQUID NITROGEN TEMPERATURE

Takeo YOKOBORI* and Masahiro ICHIKAWA**

ABSTRACT

Mechanical, microstructural and crystallographic factors are involved convolutedly in macroscopic brittle fracture behavior of polycrystalline low carbon steel. In order to study not only the each factor separately in a simple case, but also the interactions of these factors, in this article the following investigations were made. (a)The effect on brittle fracture of stress gradient as induced by the wall thickness of torsion specimens and by the notch effect. (b)The temperature dependence of torsion fracture stress at low temperatures with the purpose of confirming the previous conclusion on fracture criterion for brittle fracture.

A theoretical consideration also has been attempted for another explanation of brittle fracture criterion and macroscopic brittle fracture path.

§1. INTRODUCTION

Mechanical, microstructural and crystallographic factors are involved convolutedly in macroscopic mechanical behavior of polycrystalline solids. Therefore, it is needed to study not only the each factor separately in a simple case, but also the interactions of these factors as clue to the understanding of macroscopic or overall mechanical behavior. For the case of brittle fracture of steel, such type of studies have been made on tensile and torsion fracture with uniform stress distribution at liquid oxygen[1] and nitrogen temperatures.[2)-5)] In the present paper the effect on such type of brittle fracture of stress gradient as induced by the wall thickness of torsion specimens and by the notch effect were studied. The temperature dependence of torsion fracture stress at low temperatures was also investigated in order to confirm the previous conclusion[5] on fracture criterion for brittle fracture.

A theoretical consideration also has been attempted for another explanation of brittle fracture criterion and macroscopic brittle fracture path.

* Professor of Mechanical Engineering, Tohoku University, Sendai, Japan.

** Post Graduate of Mechanical Engineering, Tohoku University, Sendai, Japan.